General Disclaimer

One or more of the Following Statements may affect this Document

- This document has been reproduced from the best copy furnished by the organizational source. It is being released in the interest of making available as much information as possible.

- This document may contain data, which exceeds the sheet parameters. It was furnished in this condition by the organizational source and is the best copy available.

- This document may contain tone-on-tone or color graphs, charts and/or pictures, which have been reproduced in black and white.

- This document is paginated as submitted by the original source.

- Portions of this document are not fully legible due to the historical nature of some of the material. However, it is the best reproduction available from the original submission.

Final Report
Oblique Focus ICCD Laboratory Evaluation
July 1, 1978 to January 31, 1982

Grant No. NSG 5277
Donald G. York, P.I.
John L. Lowrance, Technical Director

Abstract

An oblique focus intensified CCD was constructed and operated in
a vacuum system. Through collaboration with our colleagues in France, LPSP,
(Verrieres-le-Buisson) special gratings were obtained and an optical sys-
tem set up to try to model a candidate UV spectrometer, MISIG, and to
produce small enough images to test the theoretical subpixel resolution
capability of the ICCD system. The efforts were only partly successful.
Based on our results, a similar detector was built and has flown
successfully on a Princeton rocket program.

I. Introduction

In 1978, Princeton and the Laboratoire de Physique Stellaire et
Planetaire (LPSP) in Verrieres-le-Buisson, France, proposed to build for
NASA an imaging UV spectrometer called MISIG (Milieu InterStellaire et
InterGalactique--the interstellar and intergalactic medium). In response
to that effort, the subject grant was made, through Goddard Space Flight
Center, to test the proposed detector concept, as well as to make prelim-
inary investigations of the proposed optical system. The evaluation of
the electronics and optics was given priority. Therefore, no analysis was
performed of the thermal or electronic performance of the proposed package
in the Shuttle itself.

This report begins with a description of the optical configurations
(§II), proceeds to a description of the detector (§III), continues with a
presentation of the data analysis techniques (§IV), and concludes with a
presentation of the spectra obtained and analysis of the results (§V).
The conclusions are stated in §VI.

II. Optical Configurations

The proposed MISIG payload is shown in Figure 1. Light enters from the upper right as shown by horizontal arrows. It first enters a grid collimator which eliminates objects far off axis. The light proceeds to a parabolic grating, which is the telescope objective. The diffracted radiation is focused onto the detector in the lower right hand corner. The wavelength that is centered on the detector depends on the angle of incidence of the light from the target onto the objective grating. This angle is to be adjusted by Shuttle-provided pointing equipment. (The grid collimator must be rotated through $\pm 2\overset{\circ}{.}5$ to avoid vignetting.) For each angle of incidence there is a different focal point. Thus the detector must be translated along the axis of the parabolic grating.

Two layouts were devised to model this situation. As shown below, the detector is windowless and must be used in a vacuum. (The science planned for MISIG covers the region 900-1200 $\overset{\circ}{A}$.) Hence all lamps, pinholes, gratings, mirrors, and the detector had to be made remotely operable, from outside the vacuum test tank.

Figure 2 shows the optical setup used for the data primarily discussed in this report (configuration A). A holographic concave grating, normally used in a MacPherson monochromator, is placed at G on a rotating table. An H_2 lamp illuminates the pinhole at S. To avoid interference of the detector with the slit housing, a flat mirror, M, deflects the diffracted beam to the detector photocathode, P. The focal length of the grating is one meter. With perfect alignment, this system is theoretically capable of producing an 18μ image at the photocathode. In practice, we are sure that the image was smaller than 30μ.

Figure 3 shows the second setup (configuration B). A spherical mirror M, produces collimated light from the pinhole at S. The beam strikes an aspherical grating and is focused on its optical axis onto the detector. It was decided that a special aspherical holographic ruling would give better images (i.e., the rulings are corrected for astigmatism). A grating was purchased from Jobin-Yvon and used in optical tests in France (see below). Attempts to use it in the Princeton failed because of aberrations in the spherical mirror. A more complicated optical system could not be constructed under the grant.
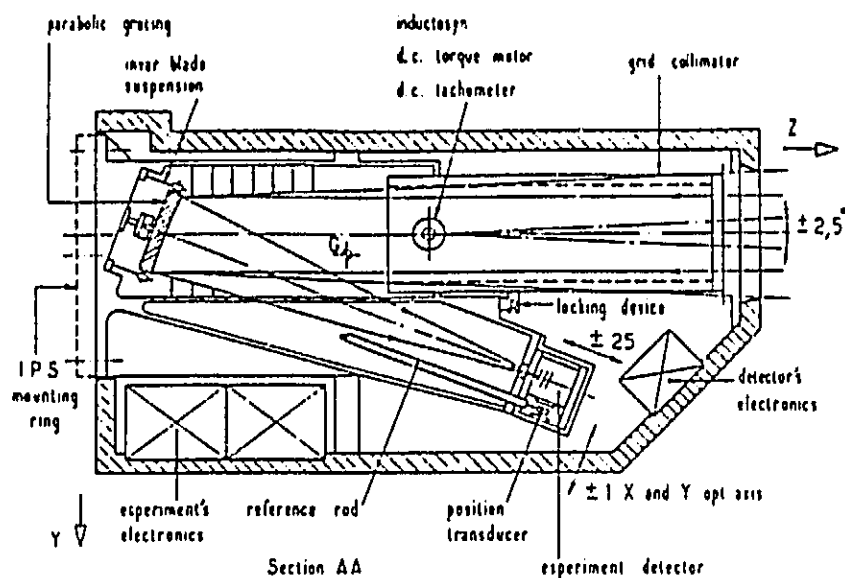
Figure 1 :Diagram of the MISIG instrument
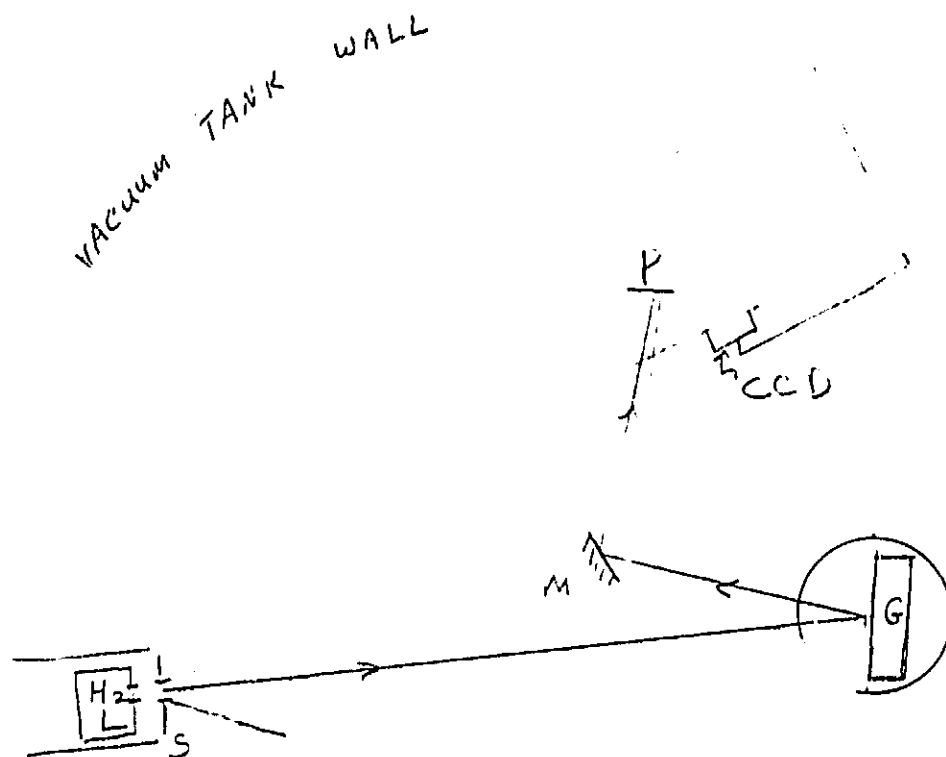
VACUUM TANK WALL

P

CCD

M

H₂ L

S

G

Figure 2: Optical configuration A showing the light path for most results reported here. Path is from the H_2 lamp L through a small pinhole (10μ) at S, to concave grating G. to mirror (flat) M, to photocathode, P. The location of the CCD in the oblique focus tube is shown.
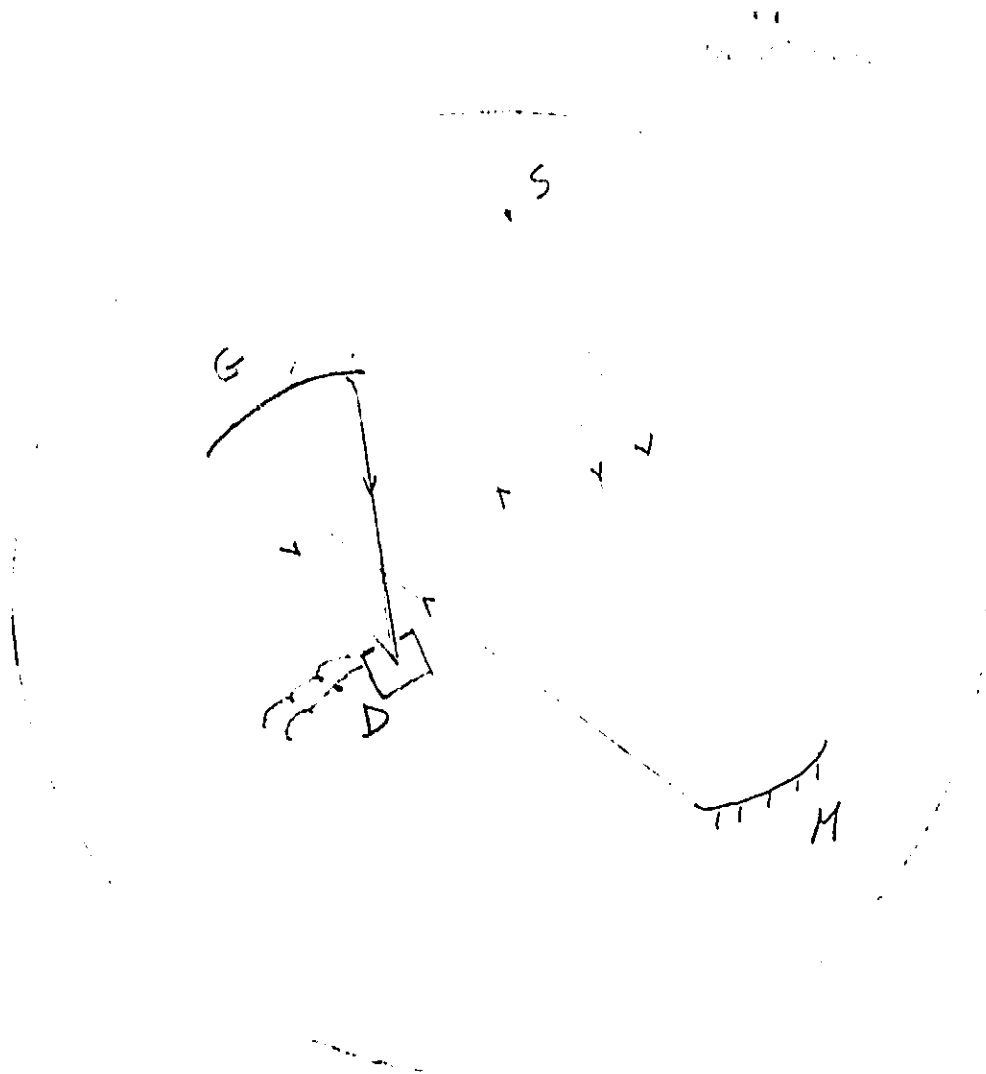
Figure 3: Configuration B, showing the light path from slit S to mirror M to aspherical grating G to detector D.

III. The Detector

The windowless image intensifier configuration used to experimentally evaluate the oblique magnetic focus concept is shown schematically in Figure 4 and a photograph of the actual test assembly is shown in Figure 5. The magnetic field is provided by long bar magnets arranged to form a 12" long cylinder borrowed from NRL, George Carruthers. The magnetic field is directed along the axis of the cylinder. The electrostatic image section shown in Figure 6 is mounted with its axis at an angle to the magnetic field using a large fiber glass plate cut in an oval shape. See both Figures 5 and 6. The CCD is mounted in a liquid nitrogen cooled housing made of copper. The CCD is located behind the window cut in the copper housing visible in Figure 3. The photocathode is located on the axis of the image section and the axis of the magnetic focus assembly. The metal plate holding the photocathode has been removed in Figure 6 to make the CCD housing visible. The ultraviolet light beam enters the image section alongside the CCD housing. This test assembly is placed in a large vacuum tank with fittings for piping in the LN_2, high voltage (22KV) to the image section electrodes and electrical connections to the CCD. Controlled boiling of the LN2 allows the CCD temperature to be controlled. We operated at $-100°C$.

The CCD Camera electronics were located outside the vacuum. The video signal from the CCD is digitized and recorded on magnetic discs and/or magnetic tape for subsequent data reduction where the single photo electron events are identified. The charge from single events appearing in adjacent pixels is summed to generate histograms of the pulse height distribution for single photoelectrons.

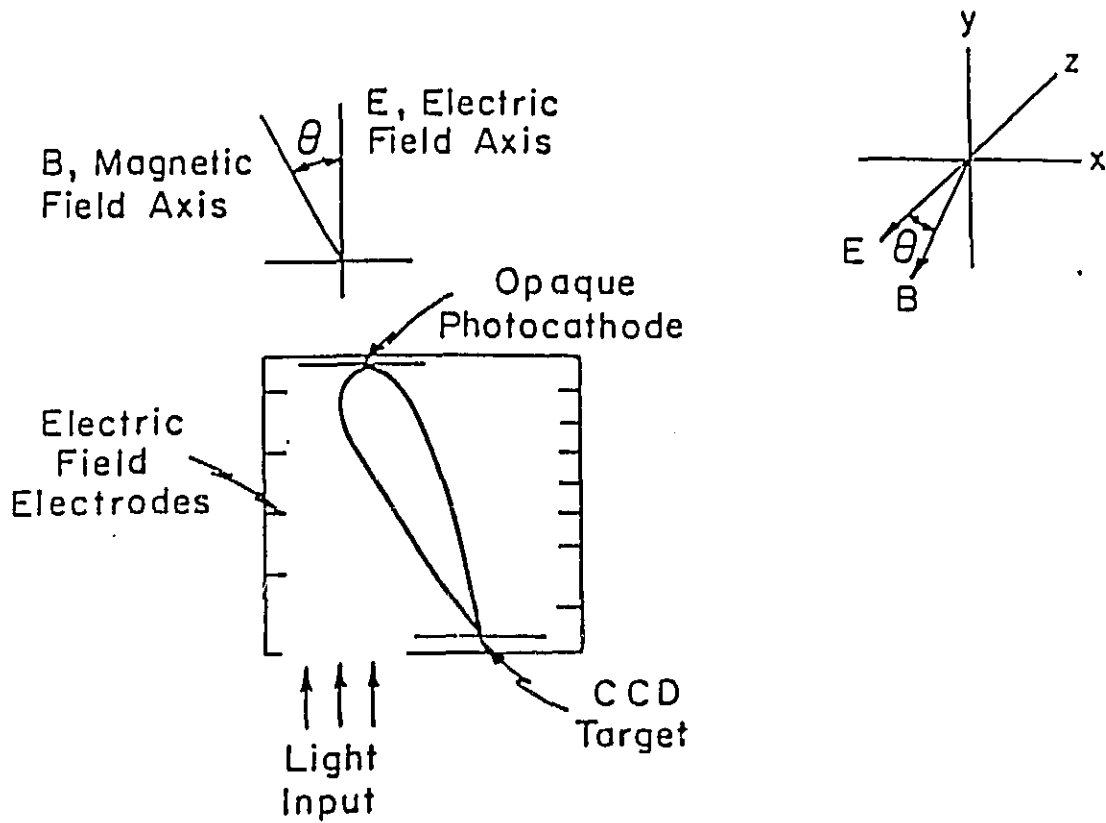The video signal is displayed in real time on an oscilloscope and TV monitor.

Figure 4 - Schematic of windowless image intensifier configuration showing oblique magnetic and electric field vectors.
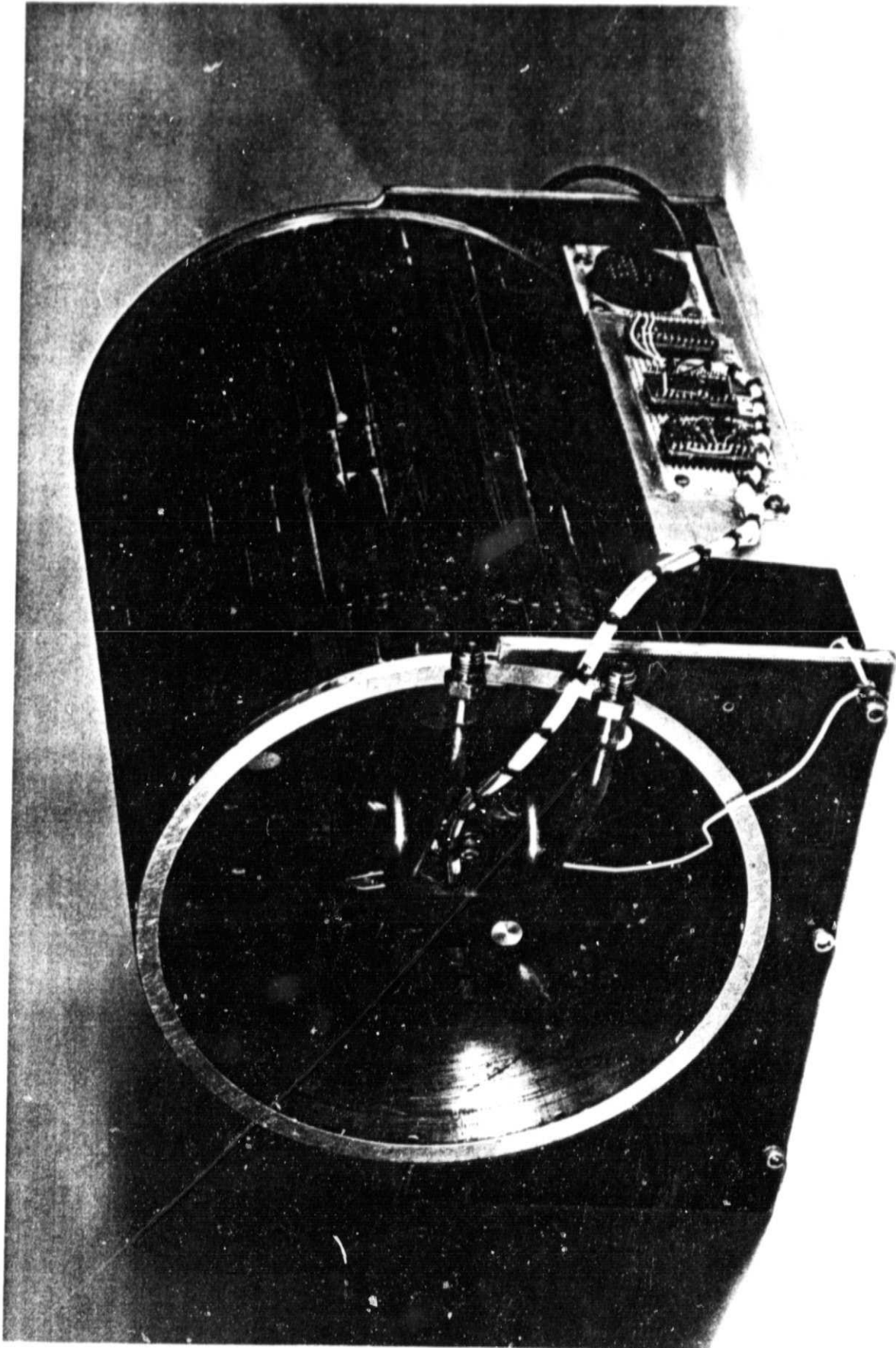
Figure 5: View of detector from the CCD end, showing cooling pipes, mounted in the permanent magnet focus assembly.
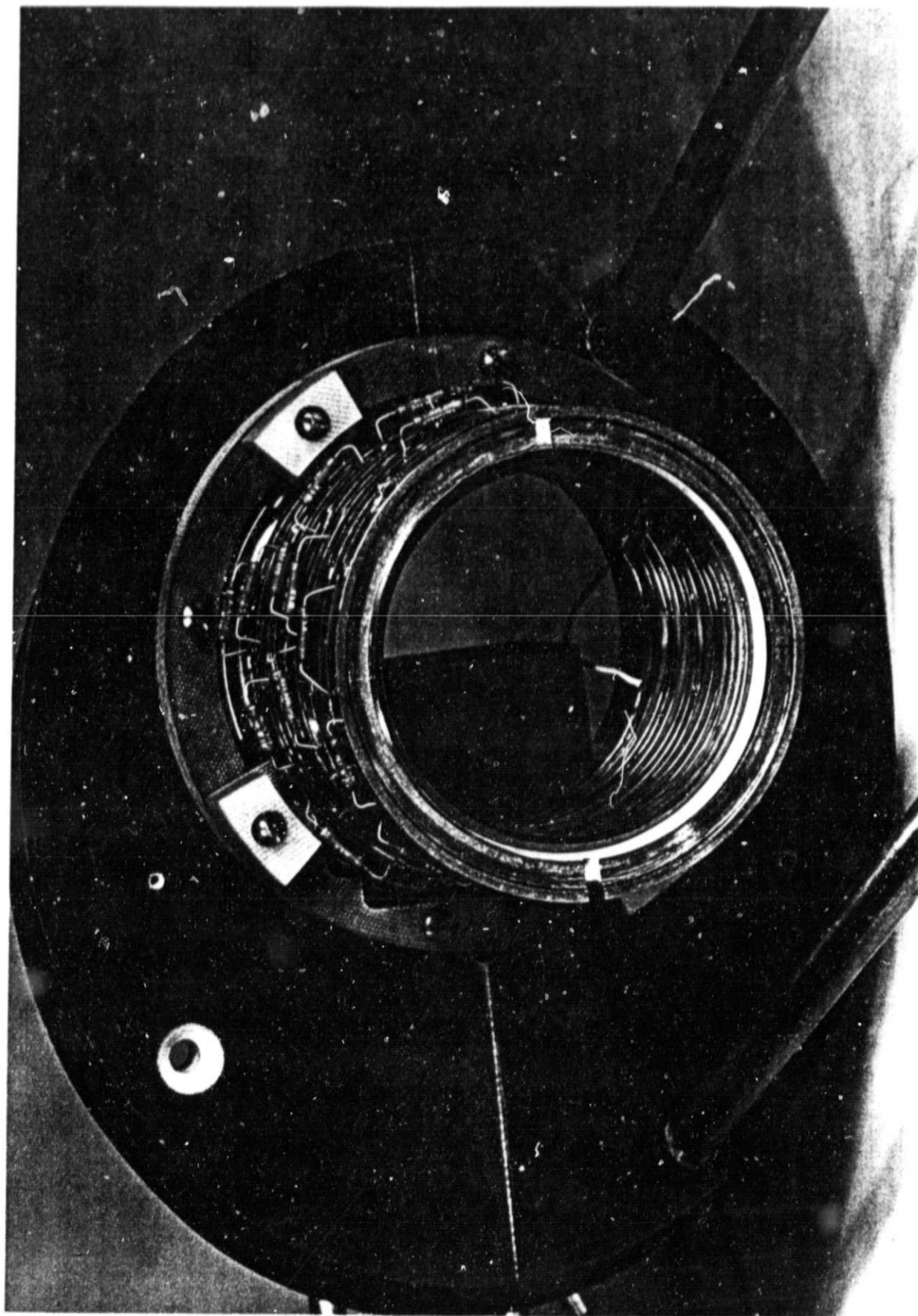
Figure 6: View of detector from photocathode end, showing electrode voltage divider resistors. The square hole at the upper left of the central annulus is where the CCD is located. The photocathode has been removed.
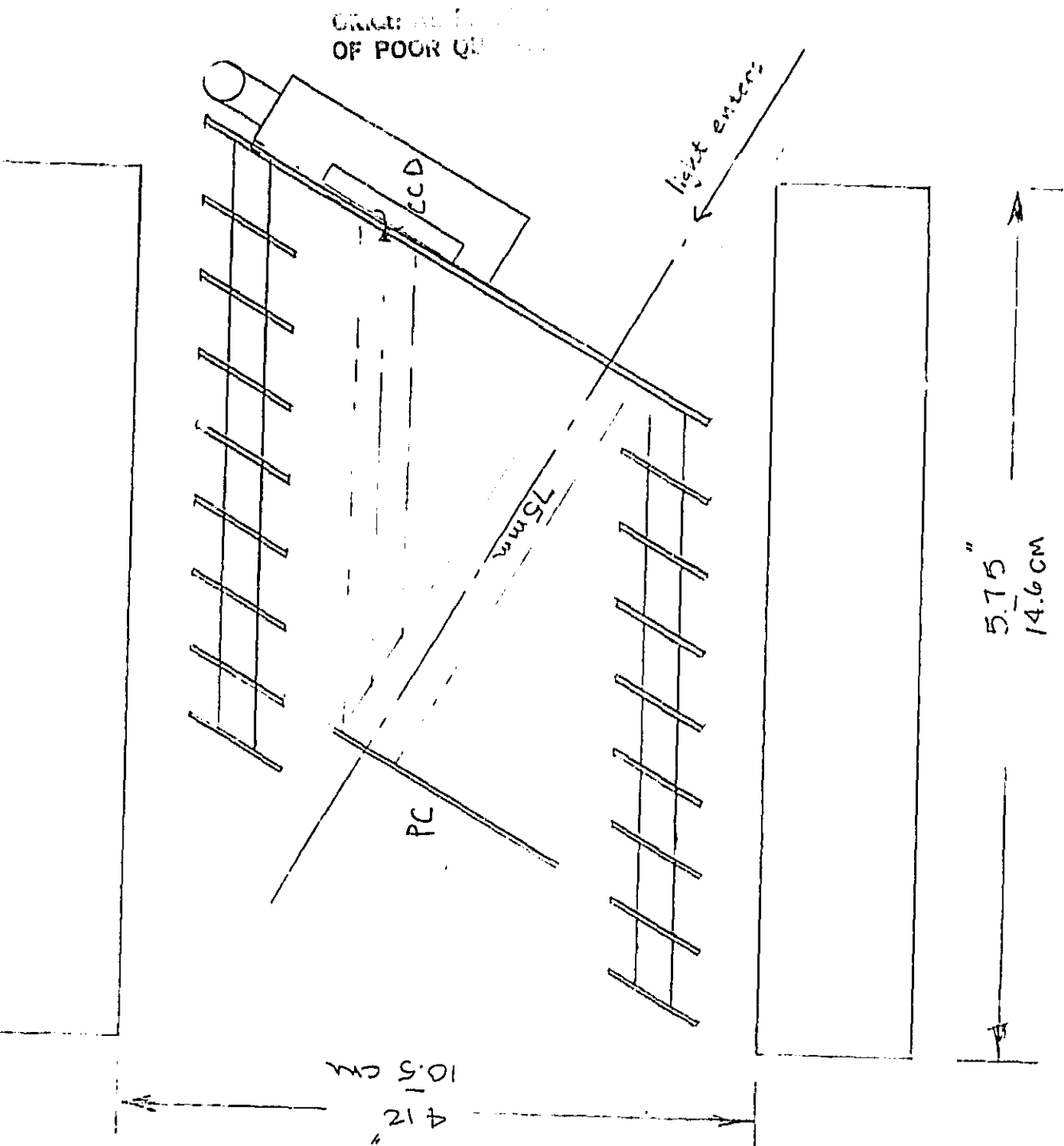
Figure 7: Dimensions of the detector.

IV. Analysis of Detector Data

The CCD was read out at a slow scan rate, one frame every 10 seconds.
The chip was masked off except for a narrow strip (oriented along the
rows). Thus, the only light to hit the device is through the strip.
Each CCD line read out passes the strip during the readout process and
during that time it can receive light. For the duration of the readout
time of 10 seconds, it is occulted. Each frame is therefore a set of
lines which record separate events without confusion, if the photon rate
is low enough (typically 1 count/sec/pixel).

Figure 8 shows a photograph of the TV screen displaying the video
output of the CCD for an entire frame time (10 seconds nominal). The
three frames show a vertical column of many dots which is the Ly α line
of HI from the "H$_2$" lamp. Each frame is at a slightly different detector
position, so the vertical column is broader on images a and c (the
detector is slightly out of focus). Each dot represents a single photon
event covering several pixels. The bright Ly α has a sufficient flux in
this setup that the dots blend together, representing multiple hits. On
all three images, two lines of dots can be seen to the right of Ly α.
These are H$_2$ lines ($\lambda 1217.35$Å at the left, $\lambda 1218.94$Å at the right).

Each photon event consists of about 6000 secondary electrons pro-
duced in the CCD for each $\jmath \jmath$ KV photoelectron coming off the photocathode.
Depending on exactly the path taken by the photoelectron to reach the CCD,
the charge of 6000 e$^-$ will be spread out over 4 – 9 pixels. Each event
must be identified and located in line and column units. Depending on the
actual position of a hit along a row, a "1" is added to an accumulating
memory for each single hit. Since the charge typically spreads out over
many pixels, the distribution of charge in the outer pixels can be used
to identify where the photoelectron hit to a resolution better than a
pixel. Each pixel was divided into five subpixels for the current work.
Each subpixel is 6μ on the detector; each pixel is 30 x 30μ. For our
experiments information along columns has no meaning (the CCD lines are
continually moving along the columns) so information on subpixels along
the columns was normally not retained in memory.

The CCD collects charge for reasons other than the arrival of photo-
electrons, Ion events may occur inside the tube. Cosmic rays or radio-
activity may lead to charge generation. There are often permanent
blemishes (bad columns or pixels). Finally, a bias voltage always exists.

Consequently, each digitized line of CCD data must have a dark frame
subtracted from it. This subtraction removes blemishes and bias voltage.
Non-repeating events (radioactivity, ion events) must be handled in a
later analysis step when events are actually labelled.

Figure 9 demonstrates the idealized result of this procedure. Figure
9a shows the video playback of 17 lines of digitized data from each of
nine separate frames of data. At the center, columns of single photon
events from Ly α and two H$_2$ lines are seen (as in Figure 8). Continuous
bright vertical columns are bad CCD columns. The very large spots at the
left (at the intersection of the ticks 1, 2, and 3) are ion events. The
The other events (of photoevent appearance) are stray photons from 1)
scattered light in the optical system; 2) events generated by dark count
emmision from the photocathode; 3) cosmic rays or radioactivity; 4) photons
from very weak H$_2$ lines that occur so infrequently that no pattern is
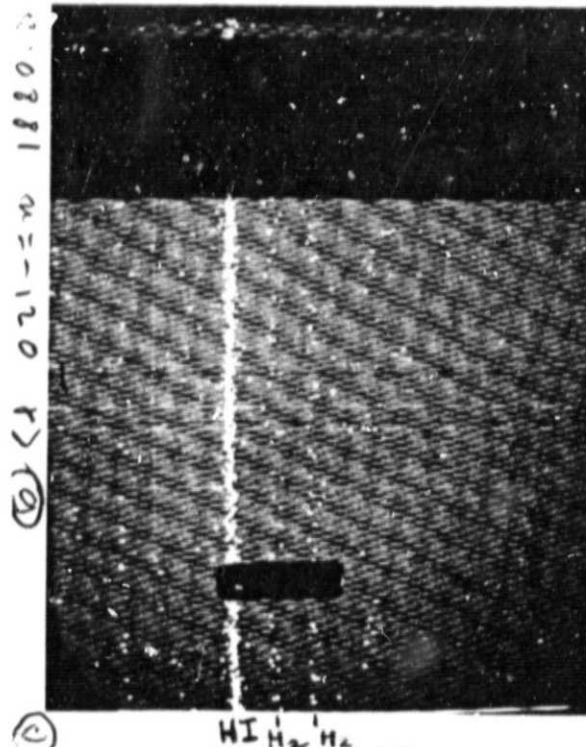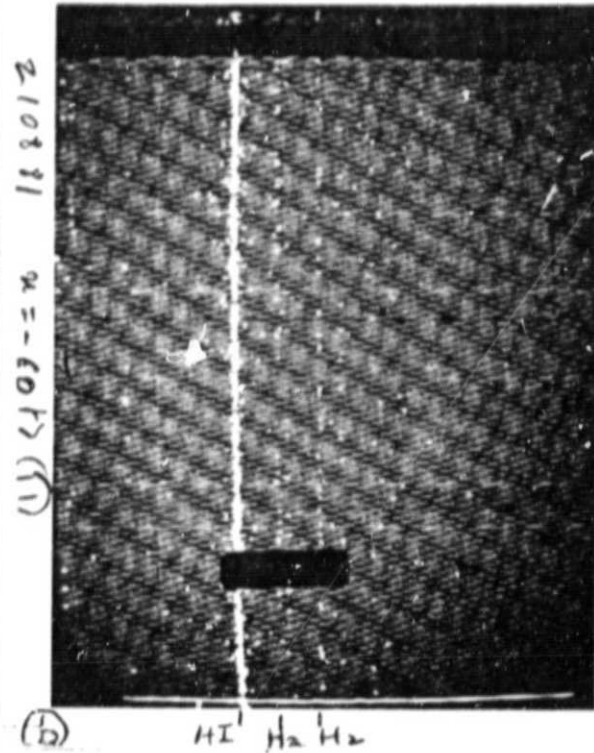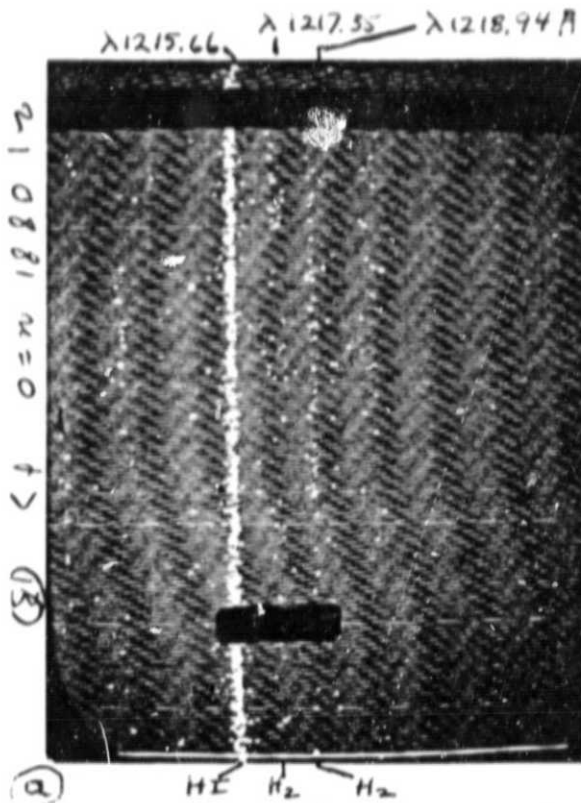discernable. Most of the events are probably in category 3).

Figure 8: Photos of the video output of three "slow scan" CCD readouts. Only a small part of the CCD (a few lines) is not masked off. During the readout, each line passes the exposure region. Any single photon events are then protected by the mask from overlapping hits for the remainder of the readout. The variable dark region at the top of each frame represent periods where the TV brightness and contrast controls were being adjusted. The rectangle near the bottom is a fiducial mark on the TV. The wavelengths of lines detected are marked in frame a
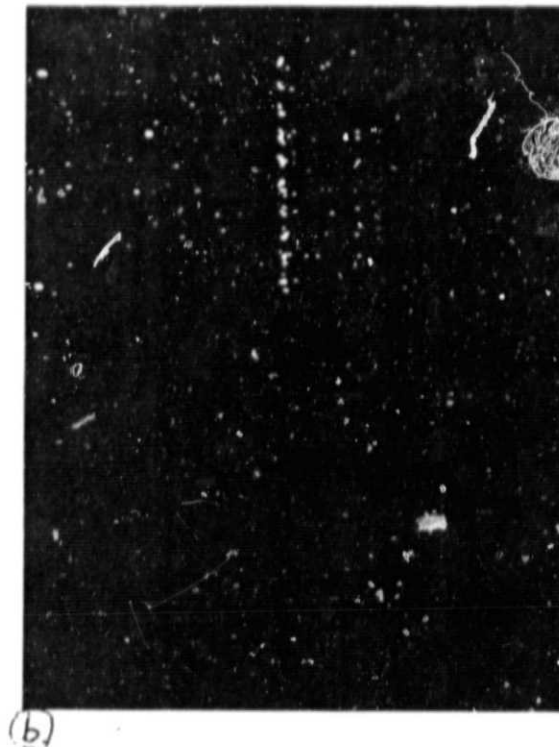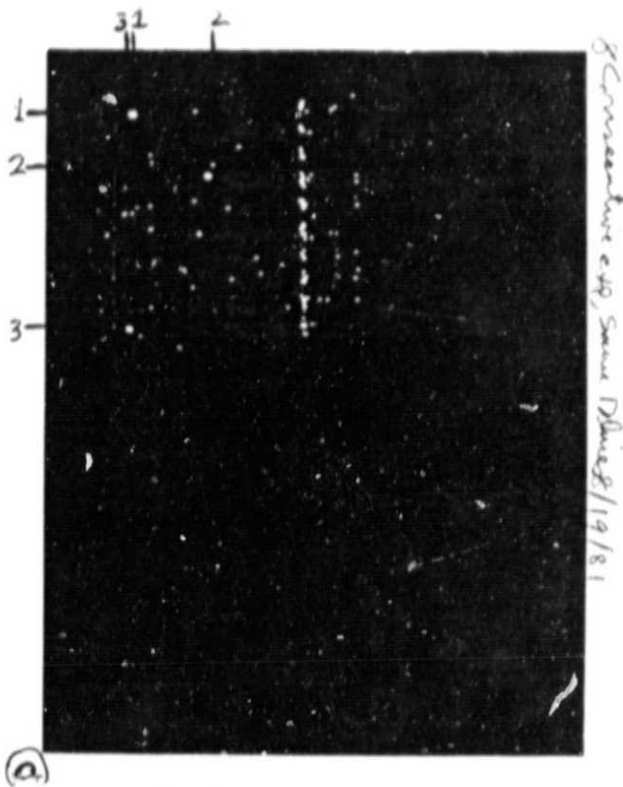
Figure 9: Photographs of video playbacks of the same 17 lines recorded in each of 9 separate CCD readout frames. The properties of the data are described in the text. Two contrast levels are shown. The photo marked (a) shows the CCD bias signal and column blemishes. After dark frame subtraction, the result in the computer should be as shown in photo (b).

The following is a detailed outline of the procedure used to isolate and centroid single events.

Program Structure

A 256 x 512 pixel section of CCD image was recorded on tape, in blocks of 'n' lines each (n=6 lines/block for our purposes).

The main program reads data one "block" at a time. A block is a group of 'p' lines, where 'p' should be greater than or equal to the diameter (in pixels) of the widest anticipated photon event ("hit"). We used p=6 for our data. The main program must have sufficient storage to keep three such blocks in core at any time (see "final processing" section for description of block usage).

Background correction: Each block, when read-in, has an average "dark frame" background subtracted from it, on a pixel-by-pixel basis. The "dark frame" background is a large array, corresponding one-to-one with the data pixels. This allows correction for the differing "dark" levels of individual pixels. In addition, a constant "mean correction" is subtracted, to account for gradual drift in the bias level. This correction (MTRIM) is calculated over one block of data, under the assumption that at least $\frac{1}{2}$ of pixels in a count histogram of the block are uncontaminated by any hit. MTRIM can be recalculated as often as desired: typically, it might be done at the start of every fifth frame (every 50 seconds).

"Hit Identification" -- Summary

1 · The "hit-nucleus" is assembled from pixels which exceed some specified threshold level (THRESH = 20 counts). A weighted-mean "center" is assigned to a hit based on the counts in each pixels of the nucleus.

2 - The total counts in the pixels in a nucleus must equal or exceed some specified level (MINCTR = 50 counts). Otherwise, the apparent "hit" is assumed to have been caused by noise and is ignored.

3 - A radius is assigned to the hit: RAD = EXTENT + RADINCR where EXTENT is maximum number of pixels in any single row or column of the nucleus, and RADINCR is some arbitrary increment to the radius.

4 - Final processing (see "Final Processing of Hits"): The positions of "good" hits are recorded in a map, and all reference to final-processed hits are removed from processing arrays.

A hit may be rejected for any of the following reasons:

    a - radii of two hits overlap -- both are marked "bad", but are retained for future comparisons;

    b - total counts in hit exceed some specified maximum (hit is assumed to be an ion event, or a superimposition of several legitimate events);

    c - radius of hit extends beyond edge of CCD;

    d - diameter of hit is too large;

    e - largest concentration of counts in row or column is at extremity of hit (this situation can occur in very noisy data).

"Hit-Nucleus" Assembly

1 - First, it is noted that a pixel which exceeds threshold level (THRESH) is located with current line.

2 - Each succeeding pixel (counts > THRESH) is examined and treated as follows:

   a - Those pixels are included in the "hit" for which the counts in succeeding pixels increase or change by fewer than 'n' counts (see below).

   b - When the pixel counts decrease by more than 'n' counts, those pixels are included which continue to decrease or which differ by fewer than 'n' counts.

   c - If, after a decrease has been flagged, and an increase of more than 'n' counts occurs, it is assumed to have been caused by a separate photon-event. The "extent" of the current hit-segment in the line is terminated at the preceding pixel. The hit-segment is then recorded in the appropriate arrays for future consideration. The newly-recognized hit-segment is then processed, starting with the preceding (lower) pixel and including the current pixel.

   d - Of course, a pixel which does not exceed the threshold always marks the end of a hit-segment within the line.

   e - The weighted-mean "center" of a hit-segment is determined, and if this matches (to within 'CTRDIF' pixels -- CTRDIF = 0.5 pixels) the weighted-mean center of an existing hit-nucleus, the arrays are updated to include the new segment in that nucleus. If no such match is found, the segment initiates a new "hit nucleus".

3 - When a new line of data makes no further contribution to a hit-nucleus, final nucleus assembly is performed. An array is created, each entry of which is the sum of the counts in one line of the hit-nucleus as determined in 1 and 2 above. Processing exactly like that in step 2 above is performed on this one-dimensional array, to check for multiple hits which are distinguishable only in the 'y' direction.

'n', as used above, is the square-root of the number of "counts" in a pixel. One count is ∿20 electrons. This corresponds to a deviation of about 4.5 sigma. 'n' is redefined whenever a pixel differs from the preceding pixel by more than 'n' counts: the new 'n' is the square-root of counts from the brighter of the two pixels in question.

Final Processing of Hits

Block usage: New lines can be considered to be read-in at 3.0 in block c (see Figure 10). As each is read, other lines shift up one. In fact, lines are read one block at a time, and line numbers are treated modulo 'n' (n lines per block). Final processing of hits is performed after reading-in and performing a preliminary analysis on the last line of the block (position 3.0 in Figure 10). When the last line of the block has been read-in, hit nuclei for positions 0.0 - 2.5 should be completely assembled. Final processing (which includes checking for overlapping radii) can now be performed on hits centered in region 0.5 - 1.5 since these can overlap only with hits centered in the region 1.5 - 2.5, by the criterion that no acceptable hit can be wider than one block. Overlap is only checked for hits which follow the "current" hit (in 'y' direction) -- it will already have been checked against those hits which preceded it. If any overlap in radii is found, both hits are
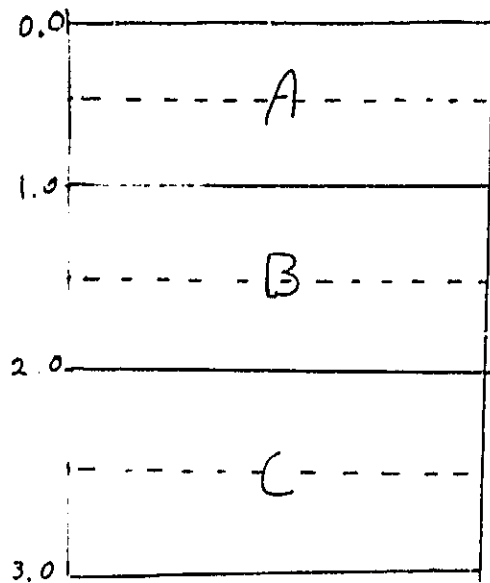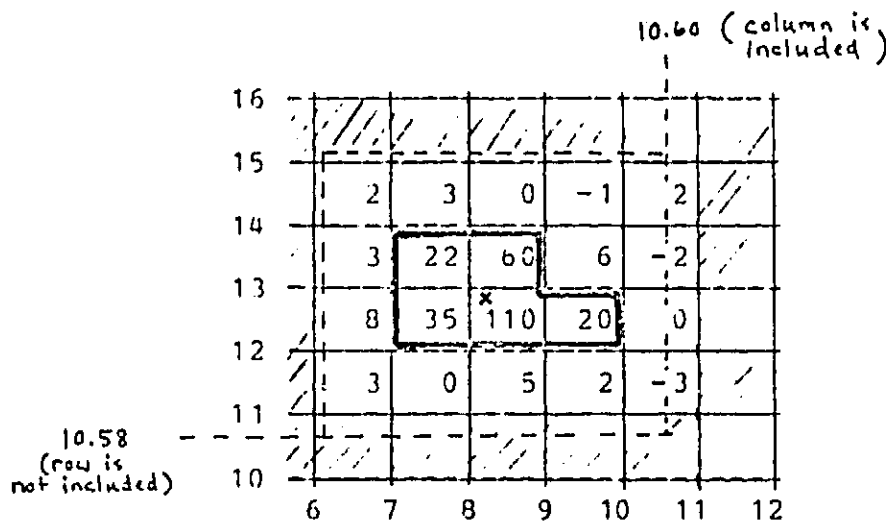
Figure 10: Block usage (see text).

Figure 11: A pattern of pixels showing a hypothetical hit with charge
spread over five pixels. The center is $\sim$ '8.35, 12.83). Therefore,
RAD = extent/2 + RADINCR = 3/2 + 0.75 = ι.   xels. The box
searched extends from x = 6.10 to x = 10.60 \.d from y = 10.58 to
y = 15.08. The total number of counts for this event is 275, so the
number of secondary electrons is 5500.

marked "bad", but are retained in the arrays for future checking.

Determination of total counts: A box is drawn around the weighted-mean center of the hit, extending RAD pixels in both x and y directions. All pixels with centers falling within this box are included in summing the total counts in the hit. An example is shown in Figure 11.

Position determination (centroiding): The column and row which contain highest fraction of total counts for the hit are found, and fractions of the hit in neighboring columns/rows are used to access a look-up table to locate the center of the hit (in x and y, respectively) more precisely within the central pixel.

In addition to final plots of the number of events per column summed over the number of frames used in each exposure, a count histogram is made. A typical example is given in Figure 12. The histogram shows the number of events with a certain number of counts recorded (one count = 20 e$^-$). The histogram was made after the frame bias was subtracted. The noise spike at < 25 cts (50σ) due to readout noise of the CCD does not show up because hits are defined to have total counts above 50(1000e$^-$). Of 1388 hits detected, only 641 were judged to be single photon events.

Figure 12 was made for a restricted range of pixels which contained a weak emission line. Figure 13 gives a histogram of pixels 110-115 (see next section), containing the very strong Ly α line. In this case, two peaks occur, the rightmost peak corresponding to double events that were not resolved. Clearly these can be reexamined for assymmetries and possibly made useful, thus increasing the dynamic range of the detector (by as much as a factor of 10).

V. Test Results

During early 1980, a special photocathode was placed in the detector with an Air Force test pattern placed on it in gold. The electron optics was focused as well as possible without the benefit of the centroiding package just described.

In June, 1980, Alfred Vidal Madjar and his staff from LPSP came to Princeton and set up the optical fixtures with John Lowrance and his staff. The various motions of detector (Princeton) and gratings, slits, mirrors, etc. (LPSP) were implemented.

The main testing in Princeton was done in August 1981, by Don York, John Opperman (technician), and Tom Gibney (computer programer), all from Princeton, and Michael Decaudin and Daniel Parisot from LPSP. Don Long and Paul Zucchino assisted when engineering difficulties arose. Paul Zucchino helped with computer aspects of the program. All detector development and testing was done under the general supervision of John Lowrance.

An H_2 lamp was used to illuminate the grating in configuration A (Figure 2). The analysis program was not implemented for real time centroiding. Various focus motions were made, and spectra were recorded at each setting. Video displays allowed the approximate focus positions to be determined.

Figure 14 shows spectra at different focus settings for pixels 110 to 195 (Ly α is just off the edge to the left). The close pairs of lines clearly become better separated as the focus is changed. The detector was here moved in the "X" direction of the tube, which, owing to the oblique focusing, leads to a slight shift in pixel number as the focus is changed. Focus position (-95, -70, -45) are in microns from an arbitrary reference. The uniform shift of the lines marked confirms that the tube artifacts are not causing confusion (the bias subtraction is working) and that real spectral features are being detected.

The best spectrum obtained is shown in Figure 15. The figure has three parts, to avoid repetition. Figure 15a shows a spectrum of an H_2 lamp recorded photographically with the new aspherical grating, at the test facilities of LPSP. Figure 15b shows a full spectrum of the H_2 lamp made at LPSP. Figure 15c shows our results for the same spectrum. Overlapping spectral regions in the respective parts of the figure are marked. Wavelengths of H_2 lines are given in Angstroms. Ly α of HI is marked. The detail at the base of Ly α is a property of the grating/lamp combination, as shown in Figure 16.

The inset in Figure 15c gives the fully centroided reductions of pixels 120-135, a plot typical of the many obtained. Sampling on subpixel scales of 6μ is apparent. The lines have FWHM of 30μ, the same as the width of individual pixels.

Attempts to combine the prototype grating, the new detector and the grid collimator, to fully simulate the optical layout of Figure 1 (MISIG) were made. Figure 15a shows the photographic spectrum recorded at LPSP. Note that the image quality degrades on both sides of the region marked B. This is because the focus is curved and results in a finite region of the spectrum being obtainable at any one time (hence, the moving collimator and translating detector in the MISIG payload).

The configuration B (Figure 3) was set up in the vacuum tank in Princeton in September, 1981. However, the collimated beam we could produce was not adequate.
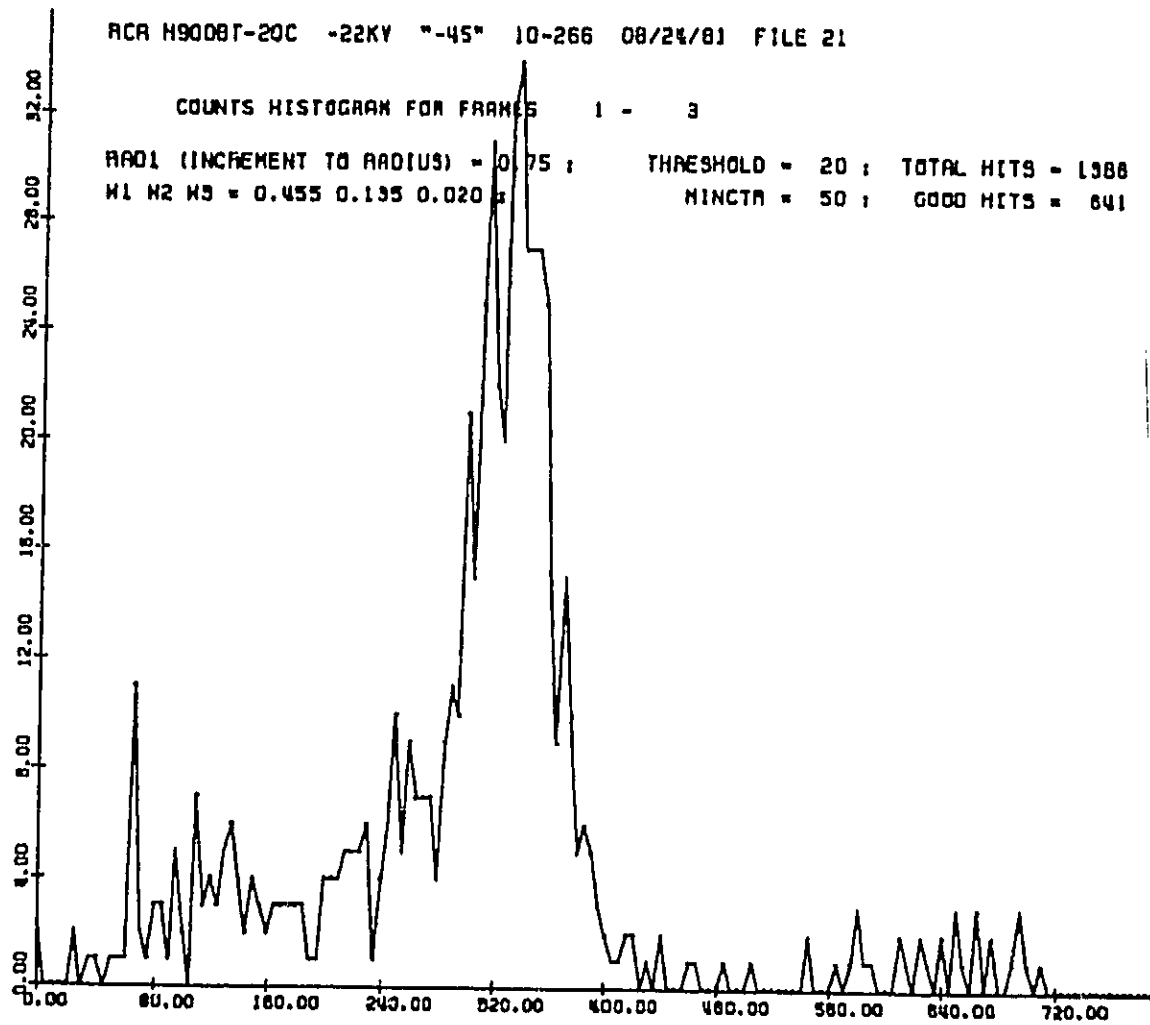
Figure 12: Histogram of _detected_ events, showing the total number of events (ordinate) at each detected count level (abcissa).
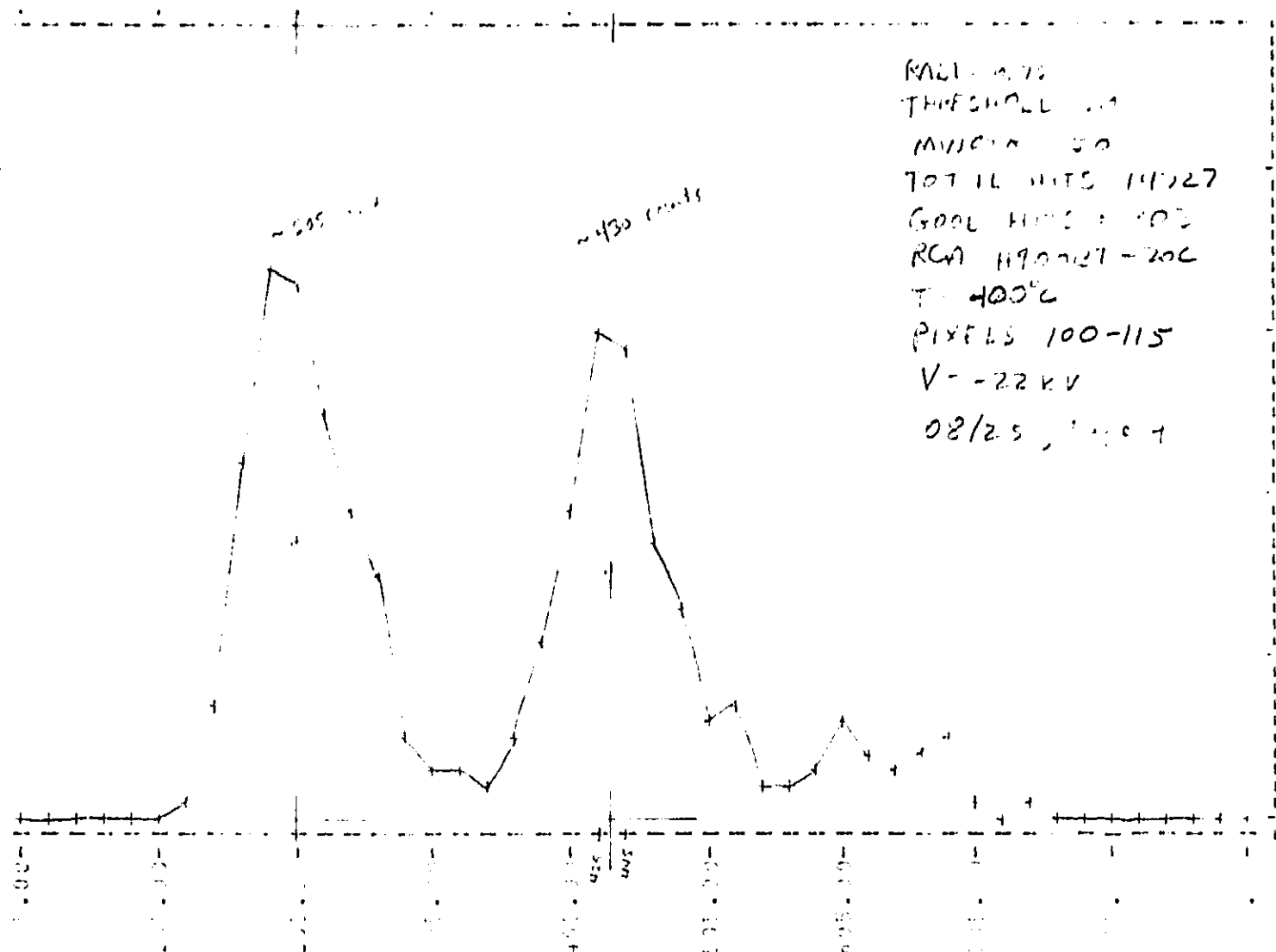
Figure 13: Count histogram for detected events in Ly α, showing the
separation of the single event and double (overlapping) event peak.
The actual number of counts in a single event differs from that
inferred in Figure 12 because the bias subtraction was done with a
constant level for the current figure, so the bias in the region of
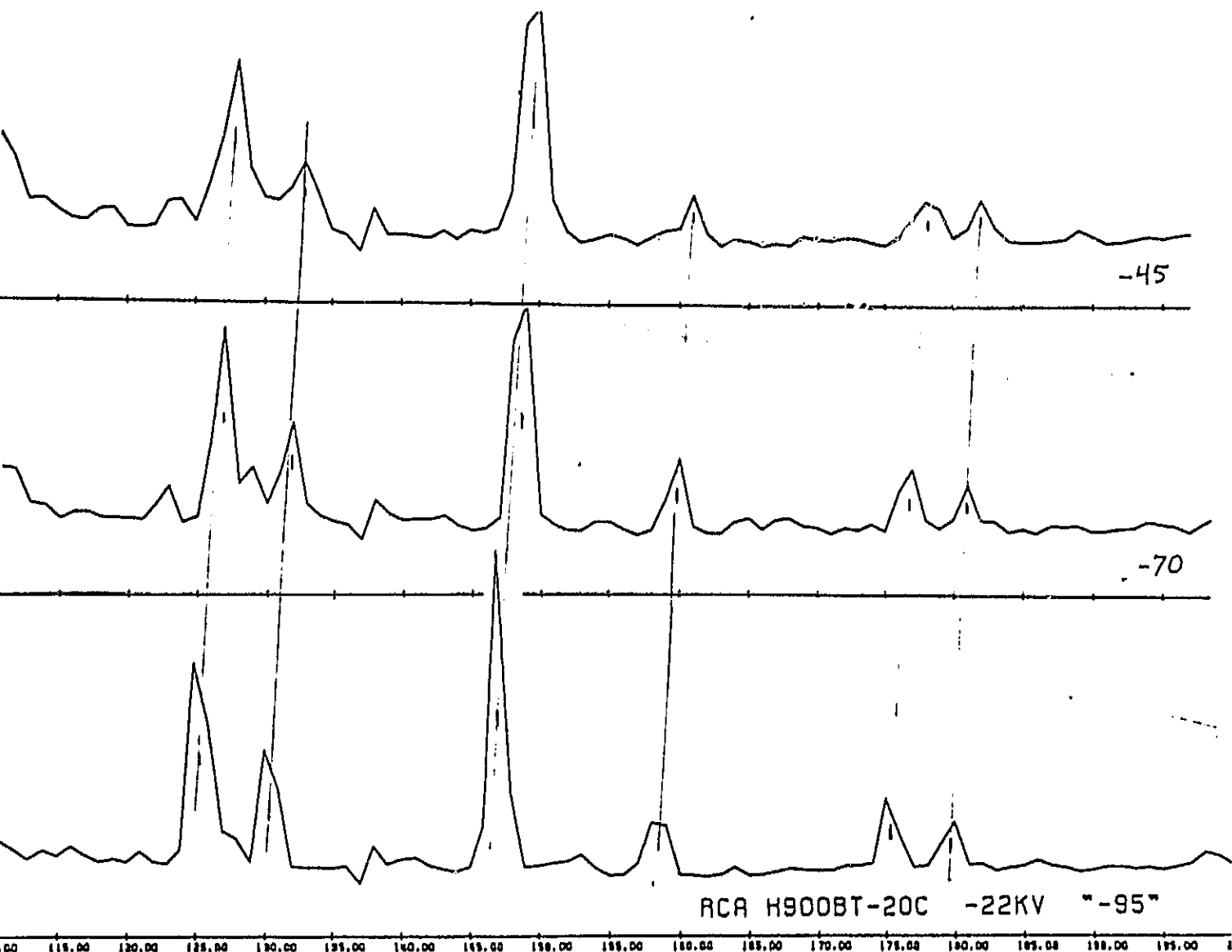Ly α was overestimated. The clean separation of the peaks is not
affected.

Figure 14: Spectra of H_2 emission lines between 1216 Å and 1221 Å for different positions of the detector photocathode. The slight scale change is caused by poor scaling of the plots and is not real. Note the different pixel number of the lines in successive plots, which eliminates uncorrected artifacts as the origin of the emission features.
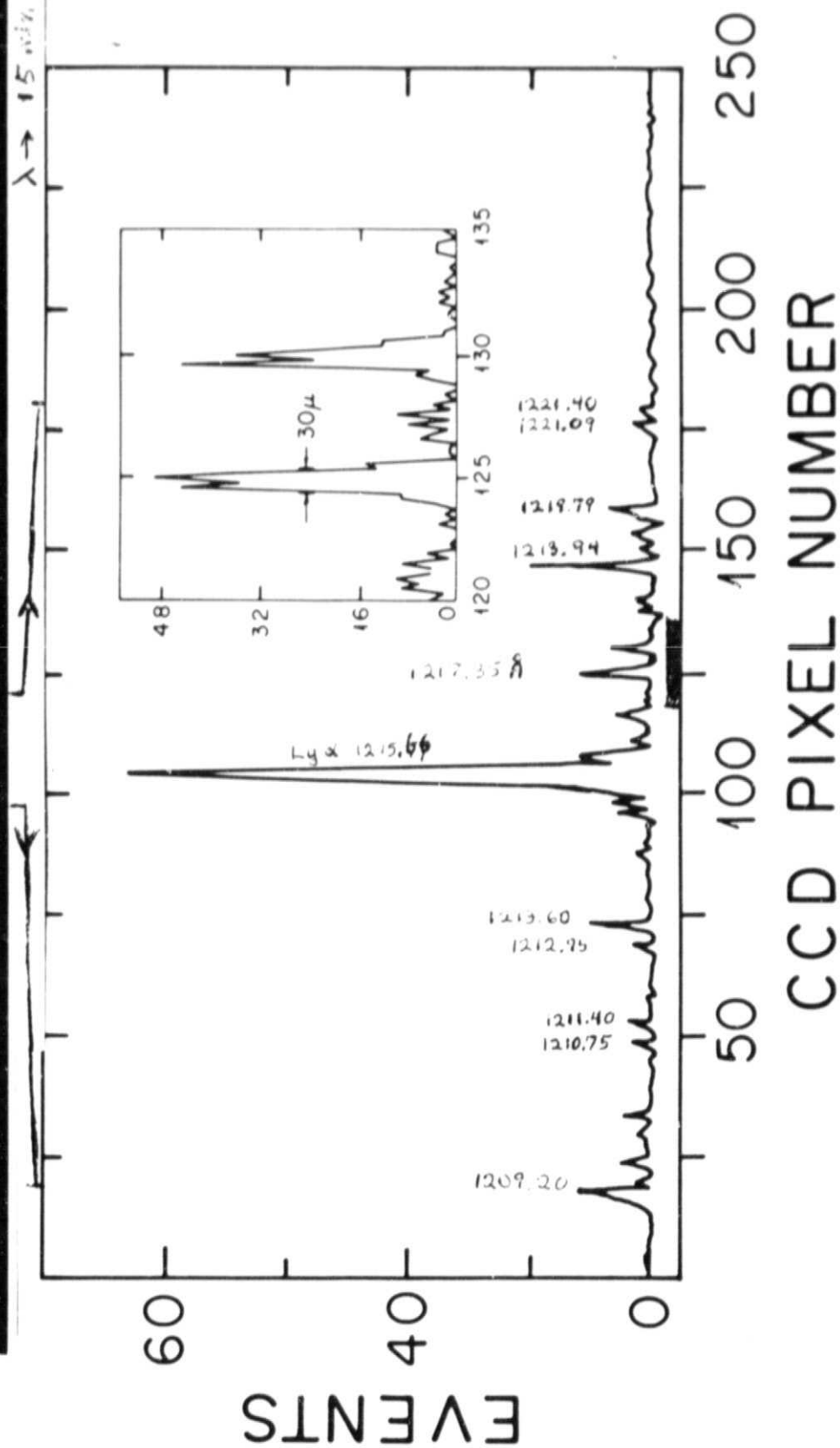
Figure 15: a) H₂ spectrum with a new aspherical holographic grating (see Figure 3).
b) Spectrum of H₂ in a stigmatic spectrograph.
c) Our recorded spectrum for 12 Å centered on Ly α (dark lines correct equal wavelength portions of a, b, and c). The inset shows full 6μ sampling for the region underlined with a bar.
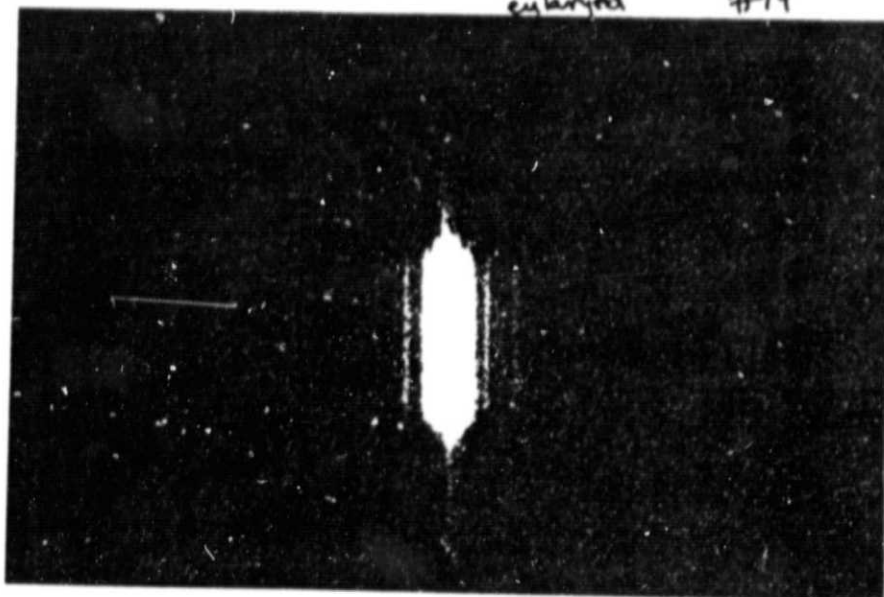
Figure 16: Blowup of Ly α from Figure 15b, showing grating ghosts and assymetry of the base. The same weak features show up in our spectra (Figure 15c).
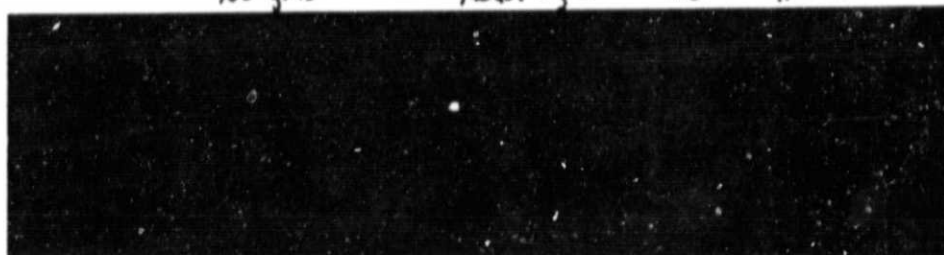

Figure 17: Image of Ly α after transmission through a grating monochrometer.

Figure 18: As in Figure 17, but with a grid collimator as the first element in the beam.

Tests with the grid collimator were also done at LPSP but could not be done at Princeton because of lack of time and funds. The grids in the collimator lead to diffraction and subsequent loss of light (or contrast for narrow lines). A mockup collimator, borrowed from Lockheed, shows this effect (Figures 17 and 18).

VI. Conclusions

The data just presented show:

a) The oblique magnetic focus ICCD is a high resolution photon counting device, capable of resolution of at least 30μ. (This performance exceeds that of microchannel/phosphor systems.) We could not convincingly demonstrate the theoretical resolution of $9-10\mu$ because of the inadequacy of our on-line reduction and subsequent inability to fully demonstrate alignment of all parts of the optical train at the time the tests were performed.

b) Virtually noiseless detection is achieved with this type of detector. (The use of the opaque photocathode from 900-1200 Å allows very high quantum efficiency -- greater than 50% -- to be achieved with no performance degradation.)

c) Reduction algorithms are straightforward and easily implemented on standard computers for the one dimensional spectral mode we chose.

d) Aspherical gratings ruled holographically can produce very high quality images ($\lambda/\Delta\lambda > 30,000$ in a one meter spectrograph) over a finite spectral range.

e) The diffraction of the grid coll'mator demands a very careful design and precise grid alignment technique, as pointed out in our MISIG proposal.

f) No impediments to constructing a fully operating MISIG were identified in the course of this work.